Quantum fluctuations in the chirped pendulum

K. W. Murch[1]*, R. Vijay[1], I. Barth[2], O. Naaman[1], J. Aumentado[3], L. Friedland[2] and I. Siddiqi[1]

Anharmonic oscillators, such as the pendulum, are widely used for precision measurement[1] and to model nonlinear phenomena[2]. Fluctuations—such as thermal or quantum mechanical noise—can excite random motion in the oscillator, ultimately imposing a bound on measurement sensitivity. In systems where equilibrium is established with the environment, noise-induced broadening scales with the intensity of fluctuations. But how does noise affect an out-of-equilibrium oscillator where the motion is varied faster than energy is exchanged with the environment? We create such a scenario by applying fast, frequency-chirped voltage pulses to a nonlinear superconducting resonator where the ring-down time is longer than the pulse duration. Under these conditions, the circuit oscillates with either small or large amplitude depending on whether the drive voltage is below or above a critical value[3]. This phenomenon, known as autoresonance, is significant in planetary dynamics[4] and plasmas[5], enables the excitation of particles in cyclotron accelerators[6] and may even be used to detect the state of a quantum two-level system[7]. Our results show that the amplitude of fluctuations determines the initial conditions of such a non-equilibrium oscillator and does not affect its time evolution.

Our oscillator is a superconducting electrical circuit based on a Josephson tunnel junction formed by two thin aluminium films separated by an oxide barrier. In response to a periodic current drive $I(t)$, the junction voltage $V(t)$ oscillates according to the Josephson relations, which describe the motion of a particle with coordinate δ in a sinusoidal potential $U(\delta) = [\hbar I_0/(2e)]\cos(\delta)$, where I_0 is the junction critical current, δ is the phase difference across the junction and e is the electron charge. This system is analogous to a mechanical pendulum with angular coordinate $\theta = \delta$ (Fig. 1a,b). The response of such an anharmonic oscillator is illustrated in Fig. 1c; as the drive strength is increased the resonant response shifts to lower frequency and ultimately exhibits bistability. In this regime, if the oscillator is excited with a constant-frequency drive of increasing amplitude, as depicted by the light-grey arrow in Fig. 1c, it abruptly switches from a low- to a high-amplitude oscillation state. This effect has been used to realize a threshold amplifier[8] to read out the state of quantum bits[9–11]. As the system is in equilibrium, fluctuation-induced switching from one oscillation state to the other is modelled as a stationary process involving escape over an effective energy barrier[12,13]. The sensitivity of this amplifier improves with decreasing intensity of noise until the quantum regime is reached[14].

The bistable regime may also be accessed by driving the anharmonic oscillator with a fixed-amplitude, chirped drive as depicted by the black arrows in Fig. 1c. For a given chirp rate α and oscillator quality factor Q, if the drive amplitude is above a critical voltage $V_c \propto \alpha^{3/4}$, the oscillator phase locks with the drive signal and climbs to the high-amplitude oscillation state[3]. Although known in plasma and accelerator physics since the 1950s, autoresonance has only recently been observed in an electrical circuit, where it was noted that this process could be used for sensitive amplification[7]. Unlike the amplitude-driven case, autoresonant excitation is by construction a non-equilibrium process, and in this letter we analyse the finite width of the threshold and the role of quantum fluctuations in determining the ultimate sensitivity of a measurement device that uses this effect.

The oscillator circuit consists of a tunnel junction embedded in the centre of a linear cavity (see Fig. 1d), realized using a capacitively isolated section of coplanar waveguide transmission line that forms a 6 GHz Fabry–Perot resonator. This architecture allows us to engineer the electrical impedance shunting the junction and hence tune the oscillator quality factor (Q), and provides a simple means to couple microwave frequency signals into and out of the oscillator. The equation of motion for the embedded system at large excitation differs from that of a physical pendulum; however, the autoresonant dynamics are unchanged[15]. We excite the circuit with a frequency chirp, created using a voltage-controlled oscillator (VCO) modulated by an arbitrary waveform generator. This signal is sent through heavily filtered coaxial lines to the chip, which is cooled to temperatures as low as 15 mK in a dilution refrigerator. The transmitted voltage is amplified at 2.3 K and demodulated using quadrature mixers at room temperature to obtain the signal magnitude relative to the drive.

We first demonstrate threshold behaviour when the oscillator is driven with a phase-continuous voltage pulse that starts at 6.075 GHz and decreases linearly in time to 5.775 GHz. The small-signal resonance frequency of the oscillator is $\omega/(2\pi) = 5.987$ GHz with $Q = 8,200$. Thus, both the start and stop frequencies are many linewidths away from resonance. The transmitted voltage ($\bar{V}$) developed in response to the drive is plotted in Fig. 2a as a function of drive frequency and amplitude. The data are acquired by averaging 5,000 frequency sweeps at a fixed amplitude and then stepping its value over a 10 nV interval. As the drive approaches the resonance condition, energy is transferred and oscillation amplitude begins to build. When the drive amplitude is weak, we observe that after a slight excitation the oscillator relaxes back to very small oscillations. On the other hand, for stronger drive, the oscillator builds up energy, behaviour that is indicative of autoresonant phase-locking of the oscillations to the drive.

A constant-frequency slice of the data in Fig. 2a, shown in the left panel, shows the threshold for autoresonance at $V_c \simeq 27$ nV. Here, the average junction voltage varies between a low level (V_l) corresponding to the unlocked events and a high level (V_h) corresponding to locked events. Within the threshold, in a given frequency sweep the oscillator either locks into autoresonance or

---

[1]Quantum Nanoelectronics Laboratory, Department of Physics, University of California, Berkeley, California 94720, USA, [2]Racah Institute of Physics, Hebrew University, Jerusalem 91904, Israel, [3]National Institute of Standards and Technology, 325 Broadway, Boulder, Colorado 80305, USA.
*e-mail: katerm@berkeley.edu.
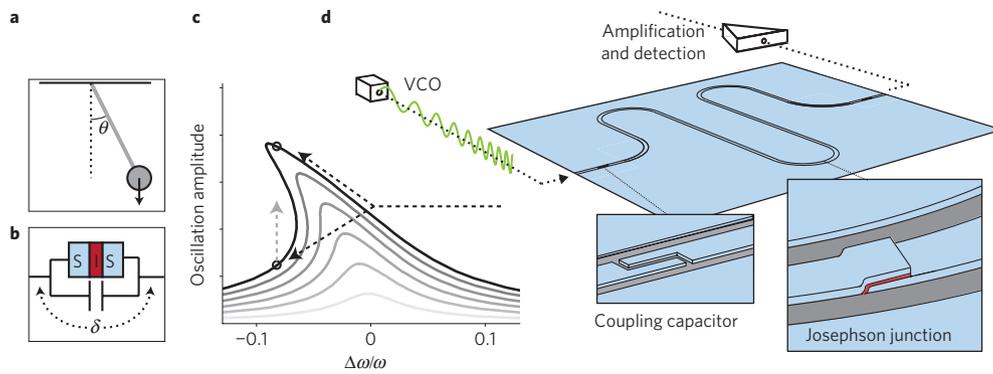
Figure 1 | The pendulum. a–c, The resonant response of an anharmonic oscillator, as realized by a pendulum (**a**) or a capacitively shunted Josephson tunnel junction (**b**), becomes increasingly asymmetric (**c**) as the drive strength is increased. Above a critical excitation the oscillator exhibits two metastable states, as indicated by black circles, with low and high amplitudes of oscillation. These states may be excited by ramping the drive amplitude at a fixed frequency (grey dashed arrow) or by chirping the drive at fixed power (black dashed arrow). **d,** Schematic diagram of the oscillator circuit consisting of a superconducting resonator embedded with a Josephson junction. The frequency-modulated drive signal is generated using a VCO and detected by means of a cryogenic amplifier and room-temperature electronics (not shown).
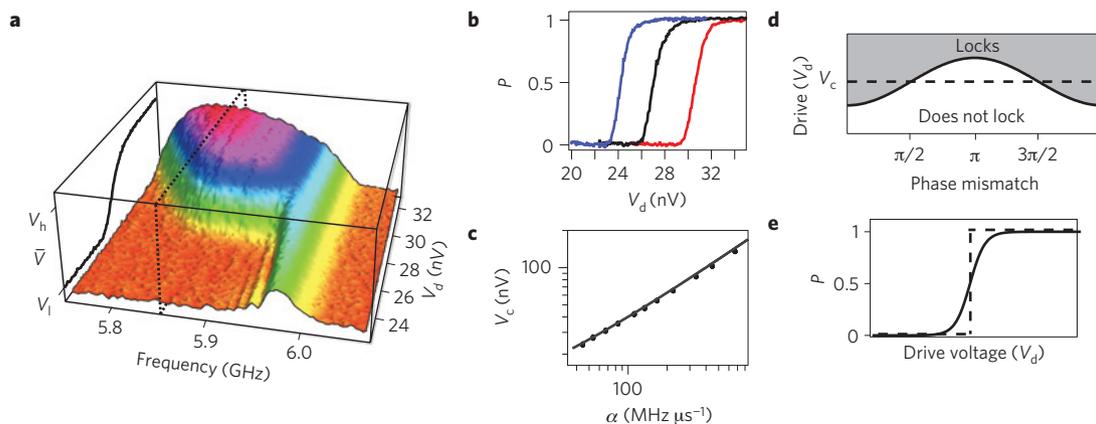

Figure 2 | Autoresonance in the chirped pendulum. a, The average transmitted voltage ($\bar{V}$) versus drive frequency and drive voltage. The drive was chirped at a rate of 50.6 MHz μs^{-1}. The dashed line indicates the fixed frequency used for the slice (left panel), which shows the threshold for autoresonance to occur at $V_c \simeq 27$ nV. **b,** The locking probability ascertained near the autoresonant threshold for chirp rates of 42.1 (blue), 50.6 (black) and 63.2 (red) MHz μs^{-1}. **c,** The threshold location, V_c, varies with the chirp rate and agrees with theoretical predictions[7]. **d,** Cartoon of the locking/non-locking regions for finite-amplitude (solid line) and zero (dashed line) fluctuation versus the phase mismatch between the drive and the oscillator. **e,** Averaging over the initial amplitudes and phases of fluctuations broadens the transition (solid line) from the zero-fluctuation (dashed line) prediction.

does not. We define the locking probability such that $P = 1$ when $\bar{V} = V_h$ and $P = 0$ when $\bar{V} = V_l$. The locking probability versus drive power is shown for three different chirp rates in Fig. 2b. The threshold location, V_c, where $P = 1/2$, is plotted versus chirp rate in Fig. 2c, and agrees with theory[7].

We now turn to the width of the autoresonant threshold. In the absence of fluctuations, the capture probability would be an infinitely sharp step at V_c as indicated in Fig. 2d,e. At the start of a chirp sequence, the resonator has an initial excitation that is the result of interactions with the fluctuating bath up to that time. The threshold for a given initial amplitude A_0 is thus either augmented or diminished depending on the initial phase mismatch, $\Delta\phi$, between the drive signal and the oscillator motion, $\tilde{V}_c = V_c - \kappa A_0 \cos\Delta\phi$, where $\kappa = 0.245$ is a prefactor determined by numerical simulations. A finite threshold width is obtained by integrating the locking probability (see Fig. 2d) over all values of $\Delta\phi$ (assumed to be uniformly distributed between 0 and 2π) and over a thermal distribution of initial amplitudes at temperature T_{eff}, where $k_B T_{eff} = (\hbar\omega/2)\coth(\hbar\omega/(2k_B T))$. We note that the quantum ground state is equivalent to a thermal distribution with $T_{eff} = \hbar\omega/2$. The threshold width, defined as the inverse slope of the locking probability at $P = 1/2$, is then

$\Delta V_c = 2\kappa\sqrt{2\pi L\alpha k_B T_{eff}}$, where L is the total inductance of the resonator and k_B is Boltzmann's constant[16].

The quantum counterpart to classical autoresonance is quantum mechanical ladder climbing. The transition between these two regimes depends on the degree of anharmonicity. When the anharmonicity is sufficiently large, high excitation is achieved by climbing the ladder of accessible states, as opposed to a continuous classical evolution[17]. To confirm the validity of our classical description when $k_B T \ll \hbar\omega$, we compute the dynamics in the presence of quantum fluctuations. The state of an oscillator can be described by its position and momentum, which for our electrical circuit correspond to the dimensionless charge (q) and current (j), respectively. In Fig. 3, we plot the Wigner quasiprobability distribution that results after the ground state—a Gaussian centred about zero—is evolved using a voltage excitation 20% greater than V_c. a–c correspond to decreasing anharmonicity with undriven energy-level shifts 100, 49 and 25 times larger than our experimental parameters. d is the classical result for the same parameters and initial conditions as in c. We observe the majority of the population in the phase-locked state, as indicated by dashed line. The data in Fig. 3c show nearly the same distribution as those of the classical calculation. For higher anharmonicity, the phase-locked
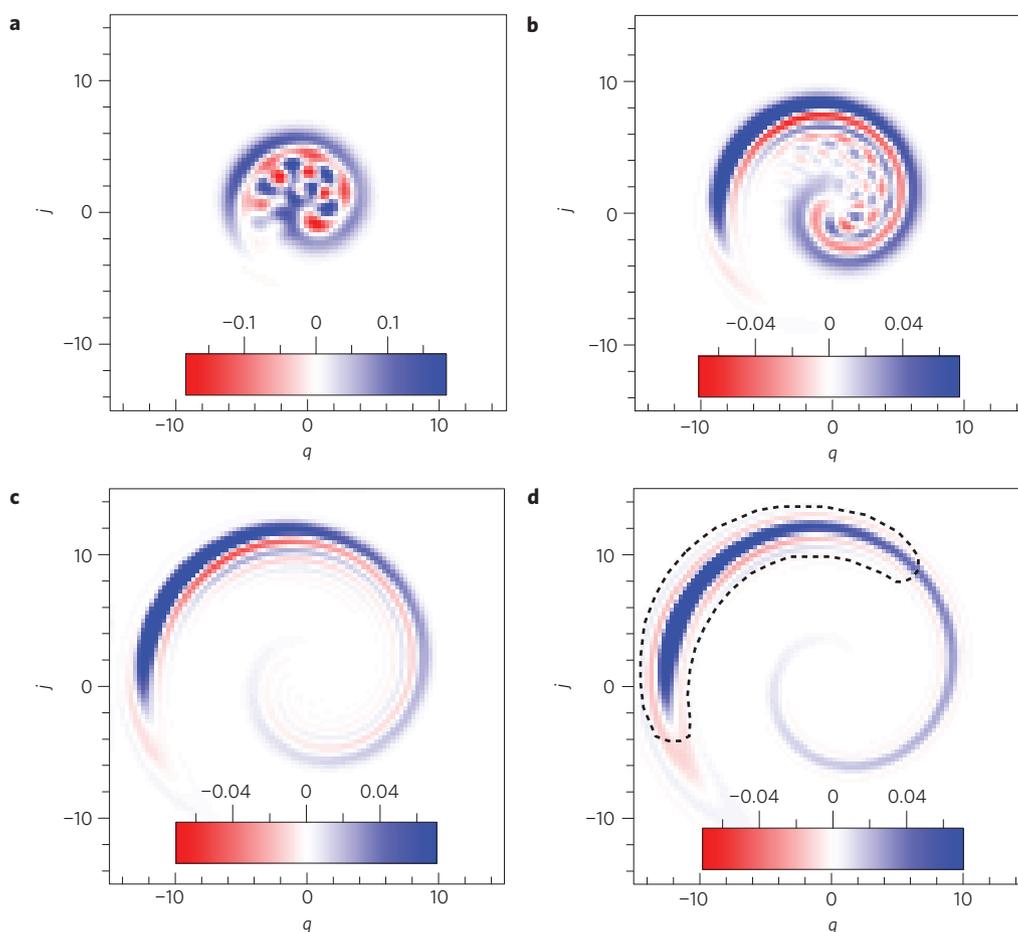
Figure 3 | Calculated Wigner distributions. a–d, Calculated Wigner quasiprobability distributions ($f(q, j, \tau = 4,215)$) for the quantum (**a–c**) and classical nonlinear oscillator (**d**) as a function of the dimensionless charge q and current j. **a–c** correspond to nonlinear energy-level shifts that are respectively 100, 49 and 25 times larger than in the experiment. The classical result in **d** shows that approximately 90% of the distribution is in the phase-locked state, as indicated by the dashed line. The tail outside this region relaxes to low amplitude if dissipation is included. Negative values in the classical calculation result from the finite accuracy of the simulation.

state remains qualitatively unchanged, but the population in the low-amplitude state exhibits a characteristic quantum interference pattern indicating the participation of a relatively small number of discrete levels. Our sample parameters, however, correspond to an oscillator with 25-times-weaker anharmonicity than Fig. 3c, and we thus expect the classical model for the transition width to be valid at all T_{eff}.

By varying the physical temperature of the dilution refrigerator we measured the transition width as a function of temperature. To compare with theory we plot the square of the transition width, scaled to temperature units as $\Delta V^2/(8\kappa \pi L \alpha k_B)$, versus temperature in Fig. 4. For temperatures above 200 mK, we observe a clear $T^{1/2}$ dependence of the width. At the lowest temperatures, saturation is observed corresponding to $T_{eff} = 144$ mK, which is precisely $\hbar\omega/(2k_B)$. The solid line indicates our theoretical prediction for the width with no adjustable parameters. To verify the quantum origin of this saturation, we plot the threshold-width data for a 1.6 GHz resonator (Fig. 4 inset). Here, we observe a $T^{1/2}$ scaling over the entire temperature range, with a suggestive flattening of the transition width at the lowest temperatures, where $k_B T \simeq \hbar\omega/2$.

Keeping the sample at $T = 15$ mK, we also injected white noise into the resonator to simulate a thermal bath. The results of this experiment are shown as the blue open circles in Fig. 4. The observed threshold width scales as $T^{1/2}$ and has an offset corresponding to the half quantum of zero-point motion of the oscillator, corroborating again a quantum-noise-broadened threshold at the

lowest temperature. Thus, quantum mechanics in our system enters only through the initial fluctuations, characterized by T_{eff}, and the system otherwise can be treated classically[18].

Our experiment is an example of the interaction of an oscillator out of equilibrium with a noise bath. The quantum saturation of the threshold width, which we note can be tuned by adjusting α, ultimately sets the resolution of a digital detector based on autoresonance. Such a detector can be used for the readout of a quantum bit. As an example, for the parameters used in this experiment a 2% variation in I_0 could be detected with unit signal-to-noise ratio in a time of ~200 ns. This compares to a typical readout based on switching between metastable states where ~1% variations in I_0 are detected in similar time[14]. In contrast to abrupt switching between metastable states[19], autoresonance involves continuous evolution to either the locked or unlocked state, raising interesting questions about the measurement back action.

Methods

The oscillator was fabricated from Al deposited on a high-resistivity Si wafer. At low excitation power, a total quality factor of $Q = 8,230$ resulted from internal losses characterized by $Q_{int} = 17,200$ and coupling to the 50 Ω environment given by $Q_{ext} = 15,800$. The critical power for bifurcation was measured to be $P_c = -123$ dBm, corresponding to a junction critical current $I_0 = 1.8$ μA and a total inductance $L = 2.3$ nH. At drive powers near P_c we observed a decrease in the total quality factor of the oscillator to $Q = 6,480$.

The chirped pulse was created by driving a VCO operating near 8 GHz with an arbitrary waveform generator and mixing it with a tone at 2.312 GHz. The
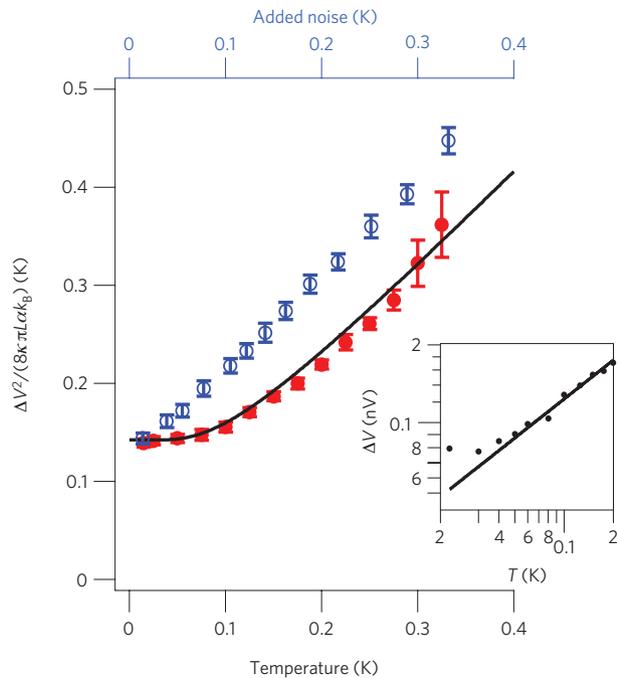
Figure 4 | The autoresonance threshold width. The square of the threshold width, scaled to temperature units as $\Delta V^2/(8\kappa\pi L\alpha k_B)$, and averaged across nine chirp rates ranging from 50 to 500 MHz μs⁻¹, versus system temperature (red circles), saturates to the value predicted for quantum fluctuations. Error bars indicate the standard error of the mean. The data are in agreement with our predictions, represented as an effective temperature, T_{eff}, and shown as a solid black line. White noise injected into the system causes the threshold width to increase $\propto T^{1/2}$ (blue open circles) with an offset given by the zero-point quantum fluctuations in the resonator. Inset: The threshold width for a junction-embedded resonator at 1.6 GHz exhibits $\propto T^{1/2}$ scaling down to $T = 40$ mK.

transmitted power from the sample was mixed with the output of the VCO to form a fixed-frequency signal at 2.312 GHz. This signal was demodulated with a local oscillator at 2.412 GHz, and the I and Q quadratures were digitized at 500 MS s⁻¹.

We modelled our oscillator by a weakly nonlinear Hamiltonian, $H = j^2/2 + q^2/2 - \beta q^4/4 + \varepsilon q \cos\phi_d$, on the phase space of dimensionless charge, q, normalized to $q_0 = j_0/\omega$ and current, j, normalized to $j_0 = \sqrt{k_B T_{eff}/L}$. The anharmonicity is given by $\beta = (\Phi_0 \omega^2 q_0^2)/(6LI_0^3)$, where $\Phi_0 = \hbar/2e$ is the flux quantum. The dimensionless drive voltage $\varepsilon = V_d/(Lq_0\omega^2)$ and the phase of the drive $\phi_d = \omega t - \alpha t^2/2$. We numerically solved the dimensionless quantum Liouville equation for the Wigner function, $f(q,j,\tau)$, where $\tau = \omega t$:

$$\frac{\partial f}{\partial \tau} + j\frac{\partial f}{\partial q} - [(q - \beta q^3) + \varepsilon \cos\phi_d]\frac{\partial f}{\partial j} = \frac{\gamma^2 \beta q}{4}\frac{\partial^3 f}{\partial j^3} \tag{1}$$

The parameter $\gamma = \hbar\omega/(k_B T_{eff})$ allows us to solve both the classical $\gamma \to 0$ and quantum $\gamma \to 2$ limits of the system (note that in the classical limit the expected temperature dependence is embedded in the reduced coordinates). We solved the Liouville equation using a standard pseudospectral method[20] for the parameters in our experiment, but for $\beta = n^2 \times 3.55 \times 10^{-6}$, $\varepsilon = 0.0246/n$ and $\alpha = 10^{-6}\omega^2$ Hz², where $n = \{10, 7, 5\}$ correspond to nonlinear energy-level shifts that are 100, 49 and 25 times that of the experiment, and drive strengths that are 20% above the autoresonant threshold. The classical evolution was approximated by solving the Liouville equation with $\gamma = 10^{-4}$.

References

1. Baker, G. L. & Blackburn, J. A. *The Pendulum* (Oxford Univ. Press, 2005).
2. Khalil, H. *Nonlinear Systems* 2nd edn (Prentice-Hall, 1996).
3. Fajans, J. & Friedland, L. Autoresonant (nonstationary) excitation of pendulums, Plutinos, plasmas, and other nonlinear oscillators. *Am. J. Phys.* **69,** 1096–1102 (2001).
4. Malhotra, R. The origin of Pluto's peculiar orbit. *Nature* **365,** 819–821 (1993).
5. Fajans, J., Gilson, E. & Friedland, L. Autoresonant (nonstationary) excitation of the diocotron mode in non-neutral plasmas. *Phys. Rev. Lett.* **82,** 4444–4447 (1999).
6. Livingston, M. S. *High-Energy Particle Accelerators* (Interscience, 1954).
7. Naaman, O. *et al.* Phase-locking transition in a chirped superconducting Josephson resonator. *Phys. Rev. Lett.* **101,** 117005 (2008).
8. Siddiqi, I. *et al.* Rf-driven Josephson bifurcation amplifier for quantum measurement. *Phys. Rev. Lett.* **93,** 207002 (2004).
9. Siddiqi, I. *et al.* Dispersive measurements of superconducting qubit coherence with a fast latching readout. *Phys. Rev. B* **73,** 054510 (2006).
10. Lupaşcu, A., Driessen, E. F. C., Roschier, L., Harmans, C. J. P. M. & Mooij, J. E. High-contrast dispersive readout of a superconducting flux qubit using a nonlinear resonator. *Phys. Rev. Lett.* **96,** 127003 (2006).
11. Mallet, F. *et al.* Single-shot qubit readout in circuit quantum electrodynamics. *Nature Phys.* **5,** 791–795 (2009).
12. Dykman, M. & Semelyanskiĭ, V. Quantum theory of transitions between stable states of a nonlinear oscillator interacting with a medium in a resonant field. *Zh. Eksp. Teor. Fiz.* **94,** 61–74 (1988).
13. Dykman, M. Critical exponents in metastable decay via quantum activation. *Phys. Rev. E* **75,** 011101 (2007).
14. Vijay, R., Devoret, M. H. & Siddiqi, I. Invited review article: The Josephson bifurcation amplifier. *Rev. Sci. Instrum.* **80,** 111101 (2009).
15. Manucharyan, V. E. *et al.* Microwave bifurcation of a Josephson junction: Embedding-circuit requirements. *Phys. Rev. B* **76,** 014524 (2007).
16. Barth, I., Friedland, L., Sarid, E. & Shagalov, A. G. Autoresonant transition in the presence of noise and self-fields. *Phys. Rev. Lett.* **103,** 155001 (2009).
17. Marcus, G., Friedland, L. & Zigler, A. From quantum ladder climbing to classical autoresoance. *Phys. Rev. A* **69,** 013407 (2004).
18. Yurke, B. in *Quantum Squeezing* (eds Drummond, P. D. & Ficek, Z.) (Springer, 2004).
19. Nakano, H., Saito, S., Semba, K. & Takayanagi, H. Quantum time evolution in a qubit readout process with a Josephson bifurcation amplifier. *Phys. Rev. Lett.* **102,** 257003 (2009).
20. Canuto, C., Hussaini, M., Quarteroni, A. & Zang, T. *Spectral Methods in Fluid Dynamics* (Springer, 1954).

Author contributions

K.W.M. and R.V. carried out the experiments and analysed the data for the 6 GHz samples. R.V. and J.A. fabricated the samples at 6 GHz and 1.6 GHz, respectively. O.N. carried out the experiments for the 1.6 GHz sample. I.B. and L.F. contributed to the theoretical understanding and calculated the Wigner distribution. K.W.M. and I.S. wrote the manuscript. All work was supervised by I.S.

Additional information

The authors declare no competing financial interests. Reprints and permissions information is available online at http://npg.nature.com/reprintsandpermissions. Correspondence and requests for materials should be addressed to K.W.M.